Int. J. Heat Mass Transfer. Vol. 32, No. 9, pp. 1671–1679, 1989
Printed in Great Britain

0017–9310/89 $3.00 + 0.00

High Rayleigh number natural convection in partially divided air and water filled enclosures

JOEL NEYMARK,† CHARLES R. BOARDMAN III
and ALLAN KIRKPATRICK
M.E. Department, Colorado State University, Fort Collins, CO 80523, U.S.A.

and

REN ANDERSON
Solar Energy Research Institute, Golden, CO 80401, U.S.A.

(*Received* 4 *August* 1988 *and in final form* 24 *January* 1989)

Abstract—This paper describes an experimental study aimed at determining the effect of internal partitions on the natural convection heat transfer across an enclosure. Experiments are conducted using a representative cubic geometry differentially heated from the side with an internal partial vertical partition. Two test cells with different working fluids are used, an air ($Pr \simeq 0.7$) and a water ($Pr \simeq 6.0$) cell. Nusselt–Rayleigh–aperture width correlation curves are developed for both the air and the water data using a resistance model. For a constant Rayleigh number, as the aperture width is decreased, the flow field undergoes a transition from a boundary layer regime to a blocked flow bulk density driven regime.

INTRODUCTION

A BASIC configuration for the study of natural convection in complex enclosures is the partially divided enclosure. In this configuration an enclosure differentially heated from the side is divided into two zones which communicate laterally across an aperture. This type of flow situation arises in a large number of engineering applications including heating and cooling of buildings, fire and smoke spread, indoor air quality and electronic equipment cooling. At high flux Rayleigh numbers ($Ra^* > 10^{10}$) thermal transport across an undivided enclosure is in the form of boundary layers which move laterally along the periphery of the enclosure. The temperature field in the core of the enclosure is uniform in the horizontal direction. When the enclosure is partially divided by a partition the flow is redirected through the interior core. The resulting transport across the aperture can be driven not only by active wall boundary layers, but also by the bulk density difference resulting from the development of a large temperature difference across the aperture.

Natural convection through apertures has traditionally been studied by either correlating the transport through the aperture with the fluid conditions on either side of the aperture, or correlating the transport through the aperture with the far wall boundary conditions. Brown and Solvason [1] developed an aperture flow model for enclosures with horizontal or vertical partitions, and correlated the aperture transport with the fluid conditions on either side of the aperture. The majority of the partially divided enclosure experiments have been conducted using water ($3 < Pr < 7$) as the working fluid, and the aperture heat transport has been correlated with the far wall boundary conditions. High Rayleigh number natural convection heat transfer measurements have been reported by Nansteel and Greif [2] for a water-filled enclosure of aspect ratio $(H/L) = 0.5$ with both two- and three-dimensional vertical partitions and wall-to-wall Rayleigh numbers (Ra) between 10^9 and 10^{11}. The three-dimensional aperture width relative to the enclosure width was held constant at 0.093, and the ratio of the aperture height to the enclosure height varied from 1/4 to 1. Nusselt–Rayleigh number data for a water-filled partially divided enclosure of aspect ratio 0.3 with a single two-dimensional partition have been correlated by Lin and Bejan [3] for wall-to-wall Rayleigh numbers between 10^9 and 10^{10}. In both of these studies the flow field was found to be laminar along the heated and cooled walls.

Natural convection experiments in air at high Rayleigh numbers are primarily limited to unpartitioned enclosures. Experimental data for air-filled partially divided enclosures is lacking. A flow visualization experiment by Olson *et al.* [4] in a full-scale enclosure at $Ra = 2 \times 10^{10}$ indicated that the boundary layer flow on the heated and cooled walls was turbulent. Turbulent temperature profiles in an enclosure at high Rayleigh number have been measured by Cheesewright and Zial [5]. Recently, attempts have been made to couple the aperture region to the wall region boundary conditions. Scott *et al.* [6] suggested that the temperature difference across the aperture was controlled by the possible blockage of the wall boundary layers by the aperture opening. They consequently found that, for water as

† Currently at Rocky Mountain Institute, Old Snowmass, CO 81654, U.S.A.

NOMENCLATURE

Ap	dimensionless aperture opening, hw/HW	T_h	temperature of hot zone at $y = H/4$
g	gravitational acceleration	dT	zone-to-zone temperature difference, $T_h - T_c$
h	height of aperture, $H/2$	DT	wall-to-wall temperature difference, $T_H - T_C$
H	height of enclosure	w	width of aperture
k	thermal conductivity	W	width of enclosure.
L	length of enclosure, $L = H$		
Nu	Nusselt number, $q''H/k(T_H - T_C)$	Greek symbols	
Pr	Prandtl number, ν/α	α	thermal diffusivity
q''	convective heat transfer/area	β	coefficient of thermal expansion
Q	convective heat transfer	ε	emissivity
Ra	Rayleigh number, $g\beta H^3(T_H - T_C)/\nu\alpha$	θ	dimensionless vertical stratification, $(T(y) - T_C)/(T(H/2) - T_C)$
Ra^*	flux Rayleigh number, $g\beta H^4 q''/k\nu\alpha$	ν	kinematic viscosity.
T_C	temperature of isothermal cold wall		
T_c	temperature of cold zone at $y = H/4$		
T_H	temperature of hot wall at $y = H/2$		

the heat transfer fluid, the temperature difference across the aperture rose sharply when the non-dimensional aperture area was reduced to below 2% of the heated wall area.

The objective of this research was to experimentally determine the flow and heat transfer characteristics of air- and water-filled partially divided enclosures at high flux Rayleigh numbers. Specific goals were to: determine under what conditions an enclosure will develop large zone-to-zone temperature differences and the resulting effect on the cross cavity Nusselt number, and to compare the behavior of small-scale water models with full-scale air enclosures.

The representative geometry studied is shown in Fig. 1. It consists of a cube with a vertical partition in the center. The partition aperture has a doorway geometry, with a height h fixed at one-half the enclosure height H, and variable width w. The thermal boundary conditions were chosen to be representative of conditions in a building interior: a constant heat flux hot wall, and a constant temperature cold wall. The other surfaces were considered to be adiabatic. Similarity between two natural convection experiments requires matching Ra^*, Pr, geometry, and the thermal boundary conditions of the interior surfaces. Rayleigh number similarity between air and water experiments can be achieved by appropriate choice of length scale and temperature difference. It is not possible to match the Prandtl numbers of air and water.

DESCRIPTION OF EXPERIMENT

Two geometrically similar apparatus were used in the experimental program. A full-scale air test cell was built at Colorado State University, and an existing small-scale water cell at the Solar Energy Research Institute (SERI) was modified for the test program. The air test cell with sides 2.44 m (8 ft) long is shown in Fig. 2. The width ratio in the air cell ranged from 1.0 to 0.009, and in the water cell from 1.0 to 0.0062. The width ratios ranged over two orders of magnitude, which made possible measurement in both the wall boundary layer, and the bulk density flow regimes. The aperture height was held constant at $h/H = 0.5$. The flux Rayleigh number in the air cell ranged from 5×10^{11} to 5×10^{12}, and in the water cell from 4×10^{11} to 1×10^{13}. The air cell Prandtl number was 0.7, and the water cell Prandtl number was approximately 6. Further information regarding experimental apparatus and procedure is given in refs. [7, 8]. A constant flux wall was constructed of eight electrical resistance heaters consisting of a graphite based heating element with an aluminum foil surface. A separately heated air gap on the exterior side of the hot wall was used to minimize direct losses from the heated wall to the environment. The electrical resistance heaters were powered by a system of variacs which were connected to a voltage regulator. The current and voltage supplied to the heaters was

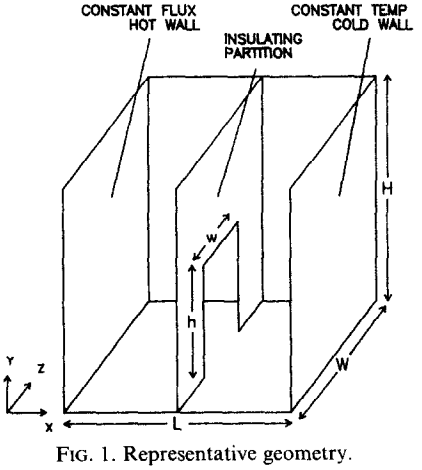

FIG. 1. Representative geometry.

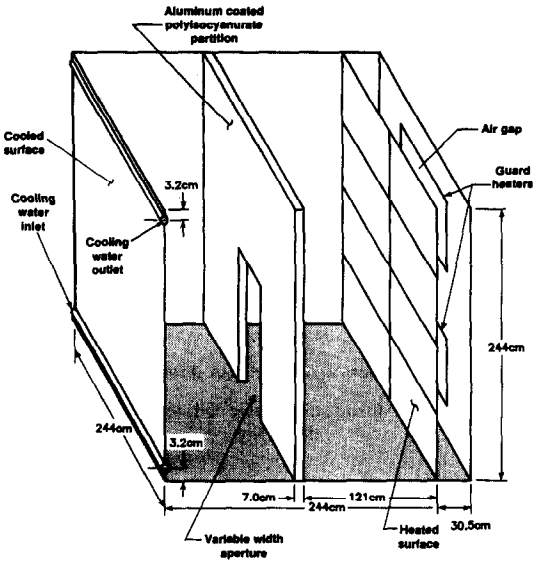

FIG. 2. Schematic of the full scale air-filled enclosure.

measured with a calibrated volt–ammeter. The power supplied to the hot wall varied from 60 to 400 W.

The constant temperature cold wall was constructed of copper solar collector absorber plates mounted on an insulated stud wall. The water flow rate was maintained at a rate such that the difference between the inlet and outlet temperatures was no greater than 0.5°C. The remaining four insulated surfaces were formed from insulated Celotex foam panels with an aluminum facing. They were insulated with 0.4–1 m thick fiberglass insulation. The partition that divided the test cell into two zones consisted of two layers of 2.5 cm thick aluminum Celotex panels that were erected parallel to the active walls. There was a 2.0 cm air gap between the Celotex panels.

The test cell was instrumented with 85 copper–constantan (Type T) thermocouples. Heat conduction through the test cell boundaries and across the partition was measured by thermocouples located on and within the test room walls, floor, ceiling and partition. The temperature difference between zones and the stratification in each zone was determined by shielded thermocouples suspended within each zone of the test cell and just outside the hot side of the partition aperture. An isothermal block was provided as a temperature reference for the test cell thermocouples. The thermocouples were calibrated to ± 0.2°C. Thermocouple voltage measurements were made with a HP3497A data acquisition unit controlled by a computer.

The external conduction heat loss from the test cell was measured over a range of input power by heating the cell with the cold wall water supply turned off. Measurements of the resulting conduction temperature profile in the six bounding surfaces were then used to determine empirical thermal conductivities for the heated wall, cooled wall, and the insulated side walls, ceiling and floor. The thermal conductivity of the dividing partition was determined using a closed partition ($w/W = 0$). For a flux Rayleigh number of 2×10^{12} and $w/W = 0.2$, $h/H = 0.5$, the external heat loss was 15% of the supplied heater power, and the partition conduction 7%. For a smaller aperture of $w/W = 0.02$, the external heat loss was 22%, and the partition conduction 16%. The variation in the local heat flux on the hot wall was estimated to be about 7%, primarily due to different vertical temperature stratification profiles between the heated air gap and the hot wall. Average local temperature variations in the cold wall were about 5% of the wall-to-wall temperature difference.

Since one of the experimental objectives was to compare the convective transport in air and water, the radiative transport in the air cell was suppressed as much as possible with the use of highly reflective interior wall surfaces. The interzonal radiation exchange was determined for each test point using a three-dimensional Monte Carlo method, MONT3D, developed by Burns and Maltby [9] which calculated exchange factors between interior surfaces. The absorptivity of the Celotex aluminum surfaces of the heated and insulated walls was 0.04 ± 0.02, and the absorptivity of the black chrome surface of the cold wall was 0.11 ± 0.02, as measured by a Gier–Dunkle D9-100 infra-red interferometer. The measured interior surface temperatures and absorptivities were used in conjunction with exchange factors for a given three-dimensional geometry to calculate the interzonal radiation exchange. An energy balance was applied to each insulated interior surface to determine the convective heat transfer to the air. For a flux Rayleigh number of 2×10^{12}, the net radiation heat transfer from the hot wall to the cold wall was 10% of the input power at $w/W = 0.2$, and 2% at $w/W = 0.02$. At these apertures, the uncertainty in the determination of interzonal radiation exchange contributes to a 5 and 1% Rayleigh number uncertainty, respectively. The net convection to the air from the floor was 3% at $w/W = 0.2$, and 5% at $w/W = 0.02$, at the representative flux Rayleigh number. The net radiation heat transfer to the partition was 2% at $w/W = 0.02$.

An existing small-scale test cell at SERI was used for the water experiments. The water test cell was also of a cubic geometry with sides of length 0.57 m (2 ft). This apparatus was equipped with a constant flux hot wall, a constant temperature cold wall, and an insulating partition with an aperture of height $H/2$ and varying width. Since this was the same apparatus used by Scott *et al.* [6] most of the details relating to construction have been already published and do not warrant repetition here. However, for the experimental work presented in this study, there were modifications to this apparatus, as well as a complete recalibration and revised operating procedure. The partition thermal conductivity was reduced by use of

2.54 cm (1 in.) thick polystyrene partitions coated with epoxy based paint and undercoated with latex paint. The partition thickness relative to the enclosure height was 0.044, compared to 0.028 for the air cell. The smaller apertures ($w/W = 0.0062, 0.0102, 0.02$) were formed from Plexiglas slots. The metal floor of the test cell was insulated from the inside with neoprene rubber sheet to reduce floor conduction from the hot wall to the cold wall. The core temperature difference was measured using differential thermocouple wiring. The power supplied to the hot wall varied from 40 to 750 W. Since this apparatus was not equipped with a voltage regulator, there were variations in total flux due to hourly voltage fluctuations. When recording steady-state points, transient fluctuations in flux were typically 4% of the total flux. Average local hot wall flux variations due to vertical conduction were 7% of the total flux. Average local temperature variations in the cold wall were typically 5% of wall-to-wall temperature difference. Hourly variations in cooling water temperature were typically 3% of the wall-to-wall temperature difference. Recalibration of thermocouples and the fluxmeter yielded temperature measurement uncertainty of ± 0.14°C, and power measurement uncertainty of $\pm 2\%$. The differential thermocouples were calibrated to measure a temperature difference with an uncertainty of ± 0.03°C. The external heat loss was about 1% of the input power, and for an aperture ratio of $w/W = 0.02$, the partition conduction was about 5%.

For both enclosures, the amount of energy convected through the aperture was calculated from an energy balance on the hot zone. The energy flux convected, q'', was found from the difference between the power input to the variacs and the heat loss by conduction through the hot zone boundaries, heat conducted through the partition, and the interzonal radiation exchange which was negligible for water. The fluid properties used in the calculations of dimensionless parameters were evaluated at the average of the area weighted temperature of the cold wall and the midpoint temperature of the hot wall. The reference temperature of the constant flux wall was its midpoint temperature (T_H).

The Nusselt number is defined as

$$Nu = q''H/[k(T_H - T_C)] \quad (1)$$

and the flux Rayleigh number is defined as

$$Ra^* = g\beta H^4 q''/(k\nu\alpha). \quad (2)$$

The temperature difference across the aperture was determined from measurements in the center of each zone at the aperture half height, and nondimensionalized by the wall-to-wall temperature difference

$$dT/DT = (T_h - T_c)/(T_H - T_C). \quad (3)$$

The uncertainties in the air cell Nu, Ra^* and dT/DT due to the cumulative effects of power, temperature and radiative property measurement uncertainties have been estimated to vary from 5 to 11%, 4 to 11%, and 2 to 170%, respectively, increasing as the aperture ratio increases. The uncertainties in the water cell Nu, Ra^* and dT/DT have been estimated to vary from 4 to 5%, 3 to 4%, and 2 to 70%. The error analysis was calculated at a confidence interval of 95% using standard random error analysis [10].

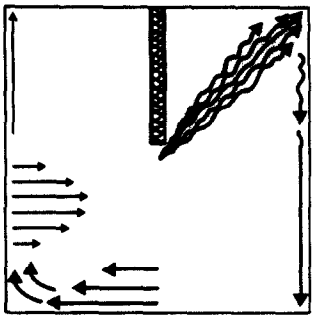

FIG. 3. Flow visualization in water cell, $w/W = 0.01$—main flow loop.

RESULTS AND DISCUSSION

Flow visualization in the water test cell using dye injection was performed at $w/W = 0.01$ and 0.2. The flux Rayleigh number was 2×10^{12}. The primary flow loop for $w/W = 0.01$ is depicted in Fig. 3. The upward boundary-layer flow along the hot wall was laminar. The hot wall boundary layer separated from the wall at $H/4 < y < H/2$. Before separation some waviness was visible in the boundary layer. The detrained boundary layer thickened and moved horizontally as shown. This horizontal flow accelerated as it moved through the aperture and exited the aperture in the form of a turbulent jet. The jet density fluctuations were visible without the assistance of injected dye and were measured by a thermocouple traverse. The jet moved toward the cold wall at about a 45° angle with respect to the vertical axis indicating a relatively even balance between buoyancy and inertia in the jet. Along the cold wall, the flow was wavy laminar with small vortices along the edge of the boundary layer.

Flow visualization studies for the 0.2 width are depicted in Fig. 4. Flow along the hot wall was characterized by a wavy laminar boundary layer. This boundary layer separated at $(3/8)H < y < (5/8)H$ and moved toward the aperture with a velocity profile as shown. After leaving the aperture and entering the cold zone, the flow rose as a laminar plume upward along the partition with a small component of entrained cooler fluid moving horizontally toward the cold wall. The plume rose to the top of the enclosure where it turned horizontally and thickened as it moved toward the cold wall. The cold wall boundary layer started out in a wavy laminar regime near the top of

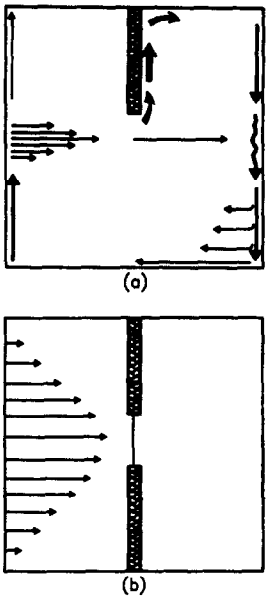

FIG. 4. Flow visualization in water cell, $w/W = 0.20$. (a) Side view, section which includes the aperture. (b) Top view, section just below midheight of the enclosure.

the enclosure ($y = H$) and grew more turbulent as it moved downward. At $y \sim H/2$ the cold wall boundary layer turbulence began to subside into wavy laminar flow.

Temperature measurements along the length of the hot wall in the water-filled enclosure were made with a thermocouple probe, at distances of 1.5 and 3 mm from the wall. The probe consisted of a 0.1 mm wire with a 0.5 mm junction protruding from a glass tube. The probe indicated no temperature fluctuations, consistent with the laminar wall flow observed with dye injection.

Flow visualization in the air cell was performed at $w/W = 0.2$, and $Ra \simeq 2 \times 10^{12}$ using isothermal smoke injection along the hot wall. The smoke particles were visible for only about 0.5 m. The boundary layer was observed to separate from the hot wall at $y \sim H/2$, the aperture height. The boundary layer on the lower half of the hot wall appeared turbulent. In Fig. 5, plots of air velocity vs time are presented for

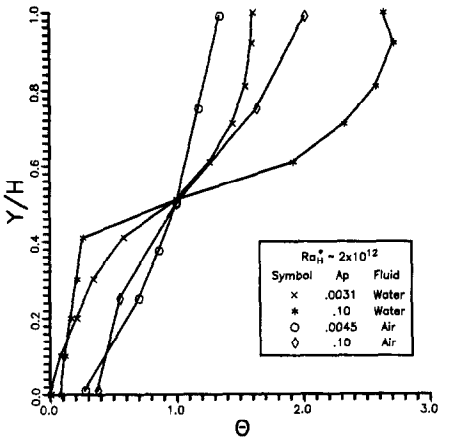

FIG. 6. Comparison of vertical temperature stratification in the hot zone of the enclosures at $Ra^* = 2 \times 10^{12}$.

selected distances (1.3, 2.5 and 5.1 cm) from the heated wall. The measurements were taken at $Y = H/4$ (the aperture half height) and for $w/W = 0.04$ and $Ra^* = 3.6 \times 10^{12}$ using a Datametrics hot-wire anemometer. The velocity fluctuations at 1.3 and 2.5 cm are characteristic of turbulent flow in the boundary layer. For the range of flux Rayleigh numbers (0.5×10^{12}–5×10^{12}) of the air experiment, the velocity measurements indicated that the boundary layer flow was turbulent along the heated wall.

A comparison of relative vertical temperature stratification for $Ra^* \sim 2 \times 10^{12}$ in the air-filled and water-filled enclosures is presented in Figs. 6 and 7 for the hot and cold zones, respectively. These data were taken along a vertical line in the center of each zone. In these figures y/H is a dimensionless height where y is the height of the data point and H the height of the test cell. The relative stratification, θ, is defined by

$$\theta = (T(y) - T_C)/(T(H/2) - T_C). \quad (4)$$

In general, the air is more linearly stratified than the water. In Fig. 6, stratification in the lower quarter of the hot zone tends to increase slightly with decreasing aperture width, whereas stratification at midheight

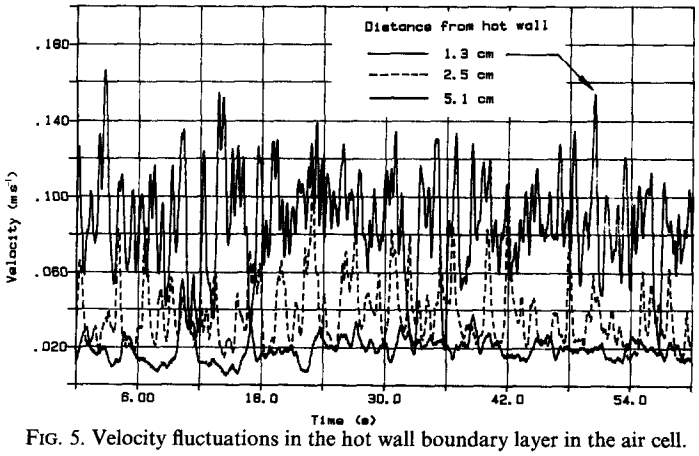

FIG. 5. Velocity fluctuations in the hot wall boundary layer in the air cell.

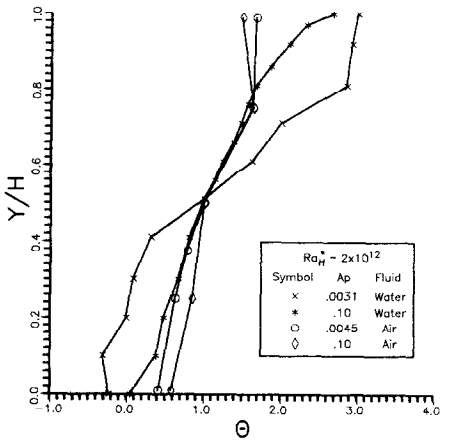

FIG. 7. Comparison of vertical temperature stratification in the cold zone of the enclosures at $Ra^* = 2 \times 10^{12}$.

and above decreases with decreasing aperture width. In Fig. 7 the water stratification in the upper half of the cold zone increases with decreasing aperture size. The relative air stratification is virtually unchanged.

The air and water Nusselt numbers are plotted vs Rayleigh number and aperture width in Figs. 8 and 9, respectively. The air Nusselt number is not a strong function of aperture width until the aperture width is less than 0.1. The corresponding aperture width for the water Nusselt number is about 0.05, which is about half as large as for the air data. The constant temperature hot wall Nusselt–Rayleigh number equation of Nansteel and Greif [2] was transformed into a Nusselt–flux Rayleigh number equation and is also plotted on Fig. 9. The constant flux hot wall curves are lower than the constant temperature hot wall correlation.

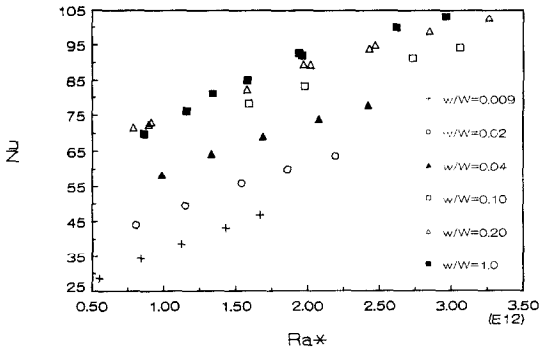

FIG. 8. Nusselt vs flux Rayleigh air data.

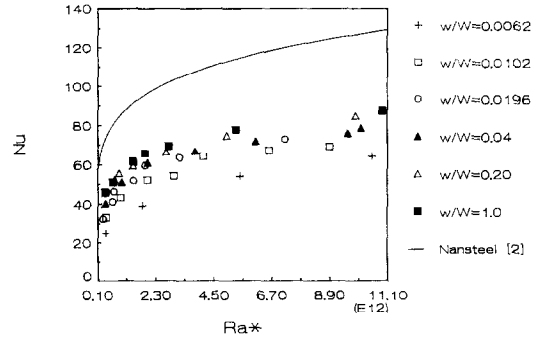

FIG. 9. Nusselt vs flux Rayleigh water data.

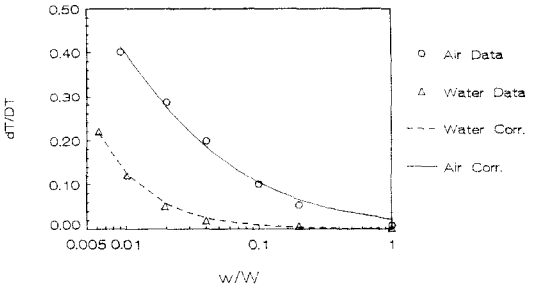

FIG. 10. Temperature difference across aperture in air and water vs aperture width at $Ra^* = 2 \times 10^{12}$.

The dimensionless temperature difference across the aperture, dT/DT, is plotted vs the dimensionless aperture width, w/W, in Fig. 10 for both the air and water data at Ra^* of about 2.0×10^{12}. This dimensionless temperature difference indicates what fraction of the total temperature drop across the enclosure occurs across the aperture. For large apertures, the temperature drop across the enclosure takes place in the boundary layers on the heated and cooled walls, and the temperature drop across the aperture is small. As the aperture size is decreased, the temperature drop across the aperture increases because of the increased aperture resistance. For a given aperture width, the air data has a greater aperture temperature difference than the water.

The air and water Nusselt numbers are plotted vs the dimensionless aperture width in Fig. 11 for both the air and water data at Ra^* of about 2.0×10^{12}. For large apertures the Nusselt number is relatively insensitive to the aperture width, since the thermal resistance is concentrated in the wall boundary layers. As the aperture width is decreases below $w/W \sim 0.05$ (water) and 0.1 (air), the Nusselt number decreases relatively sharply since the aperture resistance is increasing. These are about the same dimensionless widths at which the temperature difference across the partition begins to increase. At $w/W > 0.02$ the air Nusselt number is about 15–30% larger than the water Nusselt number. This is a consequence of the turbulent air boundary layers which cause greater heat

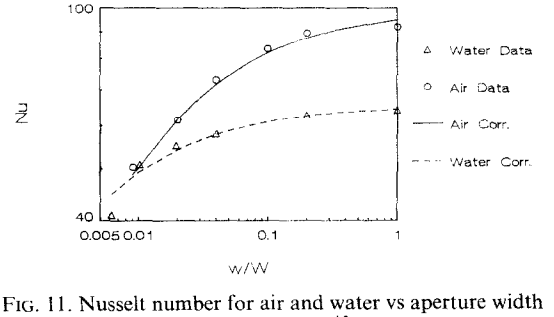

FIG. 11. Nusselt number for air and water vs aperture width at $Ra^* = 2 \times 10^{12}$.

transfer from the hot wall than the laminar water boundary layers. The difference in flow regime between air and water at the same flux Rayleigh number is probably due to the difference in Prandtl number. The effect of Prandtl number on transition is a topic worthy of future study.

The structure of the correlation equations for the Nusselt number and the aperture temperature difference can be developed from scaling analysis. The major thermal resistances are the boundary layer resistances and the aperture resistance. The cold wall boundary layer resistance scales as

$$R_C \sim 1/(kW Ra^{*n}) \tag{5}$$

where the exponent $n \sim 1/4$ for turbulent flow and $1/5$ for laminar flow. The hot wall boundary layer resistance scales as

$$R_H \sim 1/[kW Ra^{*n}(h/H)^{4n}] \tag{6}$$

since the characteristic length of flow along the hot wall is of the order of h. The aperture resistance scales as

$$R_A \sim 1/[\rho c_p (g\beta)^{1/2} w h^{3/2}\, dT^{1/2}] \tag{7}$$

$$\sim 1\Big/\left[kW\left(\frac{w}{W}\right)^{2/3} Pr^{1/3}\, Ra^{*1/3}\left(\frac{h}{H}\right)\right]. \tag{8}$$

The overall Nusselt number will then scale as

$$Nu \sim 1/[kW(R_C + R_H + R_A)] \tag{9}$$

so

$$Nu = \left[A\, Ra^{*-n} + B\left(\frac{w}{W}\right)^{-2/3} (Pr\, Ra^*)^{-1/3}\right]^{-1}. \tag{10}$$

The aperture height dependence has been absorbed into the leading coefficients since the aperture height was held constant in the experiments.

The water Nusselt number correlation equation is

$$Nu = [4.41 Ra^{*-1/5} + 5.52(w/W)^{-2/3} \times (Pr\, Ra^*)^{-1/3}]^{-1} \tag{11}$$

with a standard deviation of 4.3%. The air Nusselt number correlation is

$$Nu = [12.0 Ra^{*-1/4} + 5.08(w/W)^{-2/3} \times (Pr\, Ra^*)^{-1/3}]^{-1} \tag{12}$$

with a standard deviation of 3.9%. Please note that the exponents of the air and water correlations were fixed, taking into consideration either laminar or turbulent flow, and the resulting leading coefficients are very similar. The correlation and measured air and water Nusselt numbers are compared in Figs. 12 and 13, respectively.

The dimensionless aperture temperature difference scales as

$$dT/DT \sim Nu(w/W)^{-2/3}(h/H)^{-1}(Pr\, Ra^*)^{-1/3}.$$

The water dT/DT correlation equation is

$$dT/DT = 9.6 Nu^{0.10}(w/W)^{-1.16}(Pr\, Ra^*)^{-1/3} \tag{13}$$

with a standard deviation of 8%.

The air dT/DT correlation equation is

$$dT/DT = 5.6 Nu^{0.82}(w/W)^{-0.75}(Pr\, Ra^*)^{-1/3} \tag{14}$$

with a standard deviation of 7%. The exponent of the Nusselt number and width was allowed to vary in equations (13) and (14). The water dT/DT correlation's weak dependence on Nu is a result of the strong boundary layer flow. In water, the far wall effects have more influence on the zone temperature difference than the simple aperture resistance scaling suggests. The temperature correlation equations are compared to the data in Fig. 10.

SUMMARY AND CONCLUSIONS

Studies of the effect of variable aperture width at constant Ra_H^* show that as aperture size decreases the flow regime changes from a boundary layer to a bulk density dominated transport mechanism. These data show little change in Nusselt number with varying aperture width for $w/W > 0.1$ in air and $w/W > 0.05$

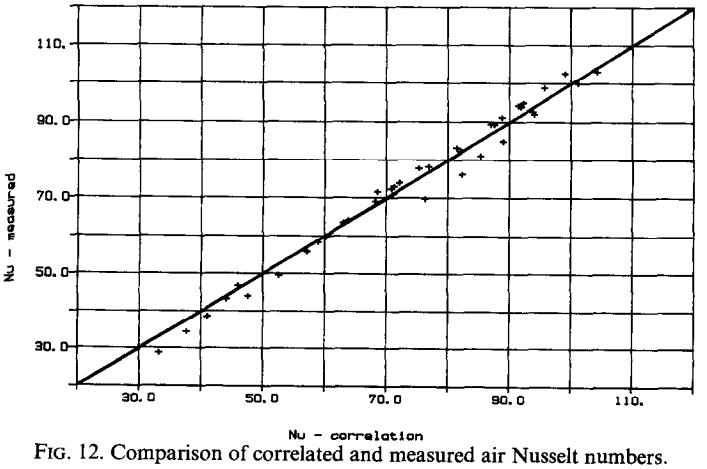

FIG. 12. Comparison of correlated and measured air Nusselt numbers.

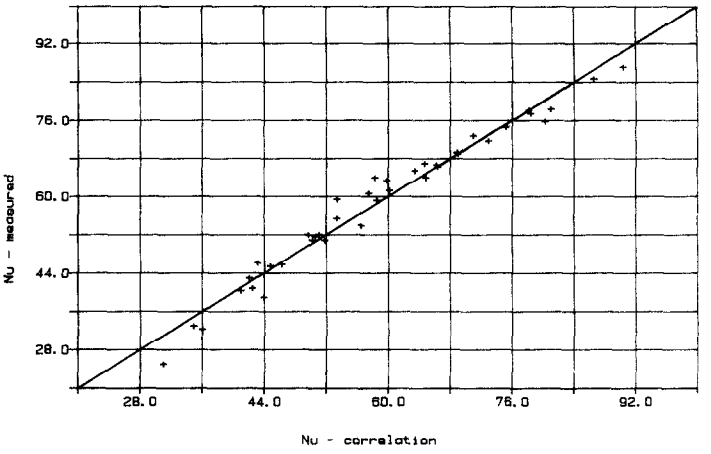

FIG. 13. Comparison of correlated and measured water Nusselt numbers.

in water. Below these values of w/W, the Nusselt number becomes a strong function of aperture width, and the temperature difference across the aperture approaches the overall enclosure temperature difference.

Differences in the behavior of air and water at similar flux Rayleigh numbers and aperture width ratios are due to the different boundary layer flow regimes along the hot wall in the two enclosures. The turbulent air boundary layer is thicker than a corresponding laminar water boundary layer. When the air boundary layer detrains from the hot wall further enlargement is expected due to turbulent mixing. The resulting horizontal boundary layer flow is then more easily blocked by the partition and also mixes better with the core which creates a situation that is more representative of a bulk density dominated transport regime. This turbulent hot wall boundary layer in the air-filled enclosure results in larger Nusselt numbers and the onset of boundary layer flow blockage at larger apertures when compared to the water-filled enclosure.

Acknowledgments—This work was supported by the Department of Energy, the Solar Energy Research Institute, and the Associated Western Universities.

REFERENCES

1. W. G. Brown and K. R. Solvason, Natural convection through rectangular openings in partitions—1, *Int. J. Heat Mass Transfer* **5**, 859–868 (1962).
2. M. W. Nansteel and R. Greif, An investigation of natural convection in enclosures with two and three dimensional partitions, *Int. J. Heat Mass Transfer* **27**, 561–571 (1984).
3. N. N. Lin and A. Bejan, Natural convection in a partially divided enclosure, *Int. J. Heat Mass Transfer* **26**, 1867–1878 (1983).
4. D. A. Olson, L. R. Glicksman and H. M. Ferm, Scale model studies of natural convection in enclosures with turbulent vertical boundary layers, ASME Winter Annual Meeting, Anaheim, California (1986).
5. R. Cheesewright and S. Zial, Distributions of temperature and local heat transfer rate in turbulent natural convection in a large rectangular cavity, *Proc. 8th Int. Heat Transfer Conf.*, Vol. 4, pp. 1465–1470 (1986).
6. D. Scott, R. Anderson and R. Figliola, Blockage of natural convection boundary layer flow in a multizone enclosure, *Int. J. Heat Fluid Flow* **9**, 208–214 (1988).
7. J. Neymark, Aperture and Prandtl number effect on interzonal natural convection, M.S. Thesis, Colorado State University, Fort Collins, Colorado (1988).
8. C. R. Boardman, Influence of aperture height and width on interzonal natural convection, M.S. Thesis, Colorado State University, Fort Collins, Colorado (1988).
9. P. Burns and J. Maltby, MONTE user's manual for MONT2D and MONT3D, Department of Mechanical Engineering, Colorado State University, Fort Collins, Colorado (1986).
10. J. R. Taylor, *An Introduction to Error Analysis*. University Science Books, Mill Valley, California (1982).

CONVECTION NATURELLE A NOMBRE DE RAYLEIGH ELEVE DANS UNE CAVITE PARTIELLEMENT DIVISEE ET REMPLIE D'AIR OU D'EAU

Résumé—On décrit une étude expérimentale destinée à déterminer l'effet de cloisons internes sur la convection thermique naturelle dans une cavité. On utilise une géométrie cubique représentative, chauffée latéralement et avec une cloison partielle verticale. Deux cellules d'essai avec des fluides de travail différents qui sont l'air ($Pr \simeq 0{,}7$) et l'eau ($Pr \simeq 6{,}0$). On développera une formule Nusselt–Rayleigh pour l'air et l'eau en utilisant un modèle de résistance. Pour un nombre de Rayleigh constant, quand la largeur de l'ouverture diminue, l'écoulement traverse une transition depuis un régime de couche limite jusqu'à un régime d'écoulement bloqué conduit par la densité.

NATÜRLICHE KONVEKTION BEI HOHEN RAYLEIGH-ZAHLEN IN TEILWEISE UNTERTEILTEN LUFT- UND WASSERGEFÜLLTEN HOHLRÄUMEN

Zusammenfassung—Das Ziel der hier beschriebenen experimentellen Arbeit war die Untersuchung des Einflusses von inneren Unterteilungen auf den Wärmeübergang bei natürlicher Konvektion in einem Hohlraum. Die Versuche wurden an einem Würfel durchgeführt, dessen eine Seite unterschiedlich beheizt wurde und in dem teilweise eine vertikale Trennwand eingebaut war. Die Versuche wurden je an einer mit Luft ($Pr \simeq 0{,}7$) und mit Wasser ($Pr \simeq 6{,}0$) gefüllten Zelle durchgeführt. Mit Hilfe eines Widerstandsmodells wurden Beziehungen für die Nusselt-Zahl als Funktion von Rayleigh-Zahl und Größe der Öffnung ermittelt. Bei konstanter Rayleigh-Zahl ändert sich das Strömungsfeld mit kleiner werdender Öffnung von einem Grenzschichtbereich in einen Bereich mit abgeschnittener Auftriebsströmung aufgrund von Dichteunterschieden.

ЕСТЕСТВЕННАЯ КОНВЕКЦИЯ ПРИ ВЫСОКИХ ЧИСЛАХ РЭЛЕЯ В РАЗДЕЛЕННЫХ НА ЧАСТИ И ЗАПОЛНЕННЫХ ВОЗДУХОМ И ВОДОЙ ПОЛОСТЯХ

Аннотация—Описывается экспериментальное исследование влияния внутренних перегородок на естественноконвективный теплоперенос через полость. В экспериментах используется полость характерной кубической формы, нагреваемая сбоку и частично разделенная внутренней вертикальной перегородкой. Используются две экспериментальные ячейки, заполненные различными рабочими средами: воздухом ($Pr \simeq 0{,}7$) и водой ($Pr \simeq 6{,}0$). При помощи понятия о термическом сопротивлении для воздуха и воды построены кривые зависимости чисел Нуссельта от чисел Рэлея, основанных на линейном размере отверстия. С уменьшением ширины отверстия при постоянном значении числа Рэлея происходит изменение режима пограничного слоя.